Microporous and Mesoporous Materials 299 (2020) 110099

Contents lists available at ScienceDirect

Microporous and Mesoporous Materials

journal homepage: http://www.elsevier.com/locate/micromeso

Separation of ethane-ethylene and propane-propylene by Ag(I) doped and sulfurized microporous carbon

Dipendu Saha [a,*], Brandon Toof [a], Rajamani Krishna [b], Gerassimos Orkoulas [a], Pasquale Gismondi [a], Ryan Thorpe [c], Marisa L. Comroe [a]

[a] Department of Chemical Engineering, Widener University, One University Place, Chester, PA, 19013, USA
[b] Van't Hoff Institute for Molecular Sciences, University of Amsterdam, Science Park 904, 1098, XH, Amsterdam, the Netherlands
[c] Department of Physics and Astronomy, Rutgers University, Piscataway, NJ, 08854, USA

ARTICLE INFO

Keywords:
Porous carbon
Alkane-alkene separation
Ag(I) doping
Pi-pi complexation
Adsorption

ABSTRACT

Separation of light olefins from their respective paraffins by adsorption is an attractive strategy due to the sustainable and inexpensive nature of adsorption process. It is well understood that the presence of Ag(I) in the adsorbent favors the adsorption of ethylene and propylene (olefins) over ethane and propane (paraffins) owing to the π - π complexation between Ag(I) and π bond present in olefins. In this research, Ag(I) doped microporous carbons were synthesized from furfuryl alcohol as carbon source. It is also shown that prior sulfurization of the carbon greatly favored Ag(I) content owing to the affinity of sulfur to Ag(I). All the carbons were successfully characterized with pore textural properties, SEM-EDX imaging and x-ray photoelectron spectroscopy (XPS). Only the carbon with highest Ag(I) content (2.5 at.%) and BET specific area (1193 m^2/g) favored the adsorption of ethylene and propylene over ethane and propane, respectively. IAST-based selectivity values were also employed to calculate binary adsorption isotherms for ethane-ethylene and propane-propylene mixtures. The IAST-based selectivity values of ethylene/ethane and propylene/propane were in the range of 4.5 to 2.5 and 5 to 2.4, respectively. Finally, column breakthrough and pulse chromatographic peaks were simulated to confirm the separation of paraffin-olefin pairs on thus carbon. To the best of our knowledge, it is the first report of the separation of light paraffin and olefins in a carbon-based adsorbent and by harnessing the π - π complexation.

1. Introduction

Separation of light olefins from their paraffin counterparts is one of the key separation needs of today [1]. Ethylene and propylene are two such light olefins and for their applications, they need to be separated from ethane and propane, respectively. The key usage of the light olefins is in the polymerization industries where polyethylene (polythene) and polypropylene are the two main polymerization products of ethylene and propylene, respectively. Besides polymers, different types of specialty chemicals are also produced from light olefins whereas light paraffins are mostly used as fuel [2]. In the last decade, the production of these olefins increased to over 50% (e.g., 25 trillion tons of ethylene per annum) [3] and with increase in demand from developing countries, the production is expected to increase further [4]. It is estimated that global annual production of ethylene and propylene has exceeded 200 million tons [1]. Usually, in petroleum industry, the olefins are synthesized by thermal decomposition, fluid catalytic cracking or thermal cracking of gas oils [5–7]. In order to meet the increasing demand of olefins, a recent technology involved the dehydrogenation of paraffin to produce olefin [8–10], however, thermodynamics constraints limited the equilibrium conversion to 20–40% [3] only. Therefore, a suitable separation is required to recover the olefins from the product mixtures. The polymer grade olefin should have a purity of11 > 99.5% in order to avoid undesirable products during polymerization.

Owing to the very similar chemical properties of an olefin with respect to its corresponding paraffin, it is very challenging to separate ethylene from ethane and propylene from propane. The kinetic diameters of ethane, ethylene, propane and propylene are 4.44, 4.16, 4.3 and 4.5 Å, respectively [12]. Owing to the very close kinetic diameter of ethane/ethylene or propane/propylene pairs, it is very difficult to separate them by size exclusion basis. However, due to the small difference in boiling points of ethane/ethylene and propane/propylene pairs (Ethane: −89 °C; Ethylene: −103.7 °C; propane: −42 °C; propylene: -47.6 °C, all ambient pressure), the most *state-of-the-art* technology

* Corresponding author.
E-mail address: dsaha@widener.edu (D. Saha).

https://doi.org/10.1016/j.micromeso.2020.110099
Received 11 December 2019; Received in revised form 27 January 2020; Accepted 11 February 2020
Available online 20 February 2020

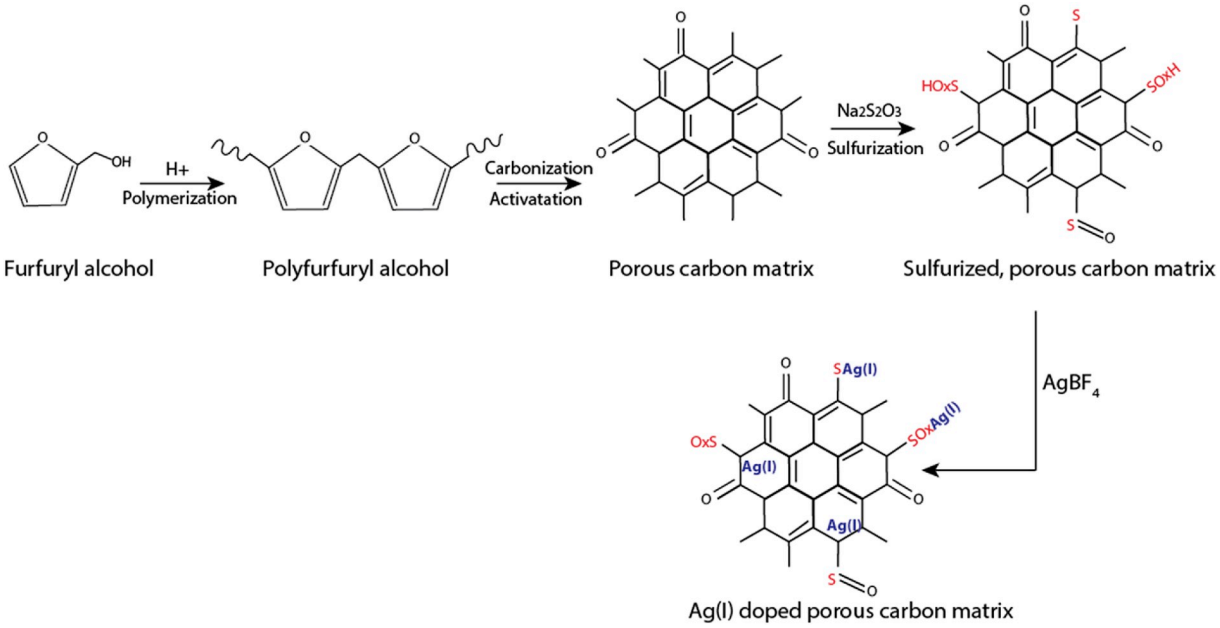

Fig. 1. Schematic of synthesis of Ag(I) doped microporous carbons

to separate light paraffin-olefin is cryogenic distillation, which has been used for almost 70 years without any significant improvement [13]. As the distillation needs to harness only a small difference in boiling point of paraffin and olefins (especially for propane/propylene mixtures) in the cryogenic region, the unit operation is performed under extreme conditions of −25 °C/23 bars for ethane/ethylene [14,15] and −30 °C/3 bar for propane/propylene separation [13] to obtain high quality and polymer grade olefins [16]. The distillation unit is also quite big, consisting of 100–150 trays [17]. Because of such operation, the Department of Energy (DOE) estimated that about 0.12 Quads (1 Quad = 10^{15} BTU) of energy was used annually for the separation of paraffin-olefin as early as 1991 [18] and it increased significantly today. A single unit of ethane/ethylene separation costs about $500 million [13]. Purification of ethylene and propylene alone accounts for 0.3% of global energy use [1], which is equivalent to the annual energy consumption of a small nation, like Singapore [19]. Because of such a large capital investment and operational cost, research is directed towards developing an inexpensive and smaller separation system that can efficiently separate light olefins from their respective paraffins. Different alternative technique that has been introduced in the separation of light paraffin and olefins are membrane separation [20–22] organic solvent-based sorbents [23] and nanoporous adsorbents [24,28].

A very large array of nanoporous adsorbents have been examined for separation of paraffin and olefins, like MOFs, zeolites or silica. As mentioned earlier, owing to similar size of the paraffin/olefin pair, affinity-based adsorption has always been a popular choice to selectively adsorb and separate the paraffin or olefins. Although few adsorbents demonstrated preference to paraffin (like ethane [12,19,24] or propane [24]), the majority of the research has been dedicated towards preferential adsorption of olefin and it mainly performed by $\pi-\pi$ complexation with the help of Ag(I) or Cu(I) species doped or grafted on the sorbent surface. π- π complexation has been implemented in different types of adsorbent systems, like, cation exchanged [25,26] or CuCl dispersed zeolites [27]. Ag(I) is often used to graft with MOFs [28] or PAFs [29] through sulfonate functionalization and the resultant adsorbents demonstrated superior selectivity towards olefins. Alumina [30], or silica [11,31] was also used to support the systems for π complexations. A detailed review of these systems can be found elsewhere [27, 32].

Although π- π complexation can influence an olefin adsorption in the mixture of olefin and paraffins, it has not been investigated for carbon-based nanoporous adsorbents. Carbonaceous adsorbents have several advantages over other adsorbents, such as easy and inexpensive synthesis method, very high and tunable surface area, high micropore volume, and remarkable chemical and thermal stability. In this research, we have synthesized a polymer-derived and highly microporous carbon followed by its sulfurization and chemical grafting of Ag(I) on its surface. This Ag(I) grafted microporous carbon was studied with adsorption of ethane/ethylene and propane/propylene pairs to investigate their separations. To the best of our knowledge, this is the first report on separation of alkane-alkene by Ag(I) doped carbon.

2. Experimental

2.1. Synthesis of Ag(I) doped and polymer derived microporous carbons

The first step of synthesizing Ag(I) doped, and polymer derived microporous carbon is to synthesize the porous carbon matrix from polymerized furfuryl alcohol, which is primarily obtained from our previous work with few modifications [33]. Typically, at first, 20 mL furfuryl alcohol (98%, Sigma Aldrich) and a solution of 0.2 g p-toluidine sulfonic acid (99%, Sigma Aldrich) in 10 mL tetrahydrofuran (THF) (99.9%, Sigma Aldrich) were cooled in an ice bath. After that, the solution of p-toluidine sulfonic acid was slowly added onto furfuryl alcohol over the course of 1 h under stirring and in ice bath. The solution was allowed to stir for five days at room temperature till a dark green colored paste of polyfurfuryl alcohol was obtained. The dark green paste was transferred onto a porcelain boat and the boat is introduced in a Lindberg-Blue™ tube furnace. The furnace was heated to 800 °C at a ramp rate of 10 °C/min under N_2 flow and then cooled down to room temperature under N_2. Thus produced polyfurfuryl alcohol derived carbon was subjected to chemical activation with potassium hydroxide (KOH) [34,35]. In order to perform the activation, 3.5 g of the carbon was mixed well with 10.5 g dry KOH (>85%, Sigma Aldrich) in a coffee grinder. The mixture was loaded onto the porcelain boat and inserted onto the same tube furnace. The tube furnace was heated in the same fashion (800 °C at a ramp rate of 10 °C/min) under N_2 (Industrial, Air Gas) gas flow and cooled down to room temperature under same N_2. The carbon was taken out from the boat and washed several times with DI water till the pH of the wash water becomes close to neutral. After that,

Table 1
Quantitative functionalities (at.%) of Ag(I) doped carbons as obtained by XPS.

Element		MC-S-Ag-1		MC-S-Ag-2		MC-S-Ag-3	
C		89.4		89.3		86.3	
O		7.1		6.6		6.7	
S	Ag_2S like	2.8	0.2	3.0	0.4	4.5	0.8
	Other		2.6		2.6		3.7
Ag		0.7		1.1		2.5	

it was filtered and dried in an oven at around 100 °C.

In order to sulfurize the carbon, we have employed sodium thiosulfate ($Na_2S_2O_3$) as sulfurizing agent according to our previous publications [36,37]. Typically, 1 g activated carbon is mixed well with 3 g or 4 g $Na_2S_2O_3$ (98%, Sigma Aldrich) in a coffee grinder. The mixture was loaded in the tube furnace within a porcelain boat in the same fashion and the furnace is heated upto 850 °C at a ramp rate of 10 °C/min under N_2 and cooled down in the same fashion. The carbon obtained so far is washed with DI water several times followed by filtration and drying. The sulfurized carbons obtained from (1:3) and (1:4) ratio of carbon to $Na_2S_2O_3$ are named as MC-S1 and MC-S2, respectively. In order to perform the Ag(I) doping, 1 g of MC-S1 is dispersed in 100 mL DI water under rigorous stirring and 2 batches of MC-S2 of the same amount are dispersed in the same fashion. The dispersion of MC-S1 and the first batch of MC-S2 were added with 1 g of silver tetrafluoroborate ($AgBF_4$, >99.99%, Sigma Aldrich) each; whereas the second batch of MC-S2 was added with 4 g of $AgBF_4$. All the mixtures were stirred for 24 h. After that, the stirring was stopped, the carbon was allowed to settle, and the water was carefully decanted. Then, 100 mL fresh DI water was added in all the batches, followed by further addition of 0.5 g fresh $AgBF_4$ in MC-S1 and first batch of MC-S2. The second batch of MC-S2 were added with 4 g fresh $AgBF_4$. All the samples underwent vigorous stirring for another 24 h. At the end, the excess water was decanted, and the carbon was washed several times with DI water. Finally, the Ag (I) doped carbon was filtered and dried in air at 100 °C. Upon Ag(I) doping, MC-S1 was termed as MC-S-Ag-1, first batch of MC-S2 as MC-S-Ag-2 and the second batch MC-S2 as MC-S-Ag-3. The overall schematic of the syntheses protocol is shown in Fig. 1.

2.2. Materials characteristics

All the Ag(I) doped microporous carbons have been characterized with scanning electron images (SEM), energy dispersive X-ray (EDX), X-ray photoelectron spectroscopy (XPS) and pore textural properties. Scanning electron microscopy (SEM) and Energy dispersive X-ray (EDX) were performed in JEOL 7500F HRDEM instrument. The pore textural properties, including BET specific surface area, total pore volume and pore textural properties were obtained in Quantachrome's Autosorb iQ-any gas surface area and porosity analyzer by N_2 adsorption at 77 K and CO_2 adsorption at 273 K. XPS data were obtained in Thermo-Fisher K-alpha instrument with monochromatic Al-Kα as x-ray source. The energy of x-ray, instrument resolution, pass energy, step size and dwell time were 1486 eV, 0.5 eV, 50 eV, 0.1 eV and 50 ms, respectively. Each sample was mounted on a carbon tape followed by irradiation with 2 eV Ar^+ ions to neutralize the charges.

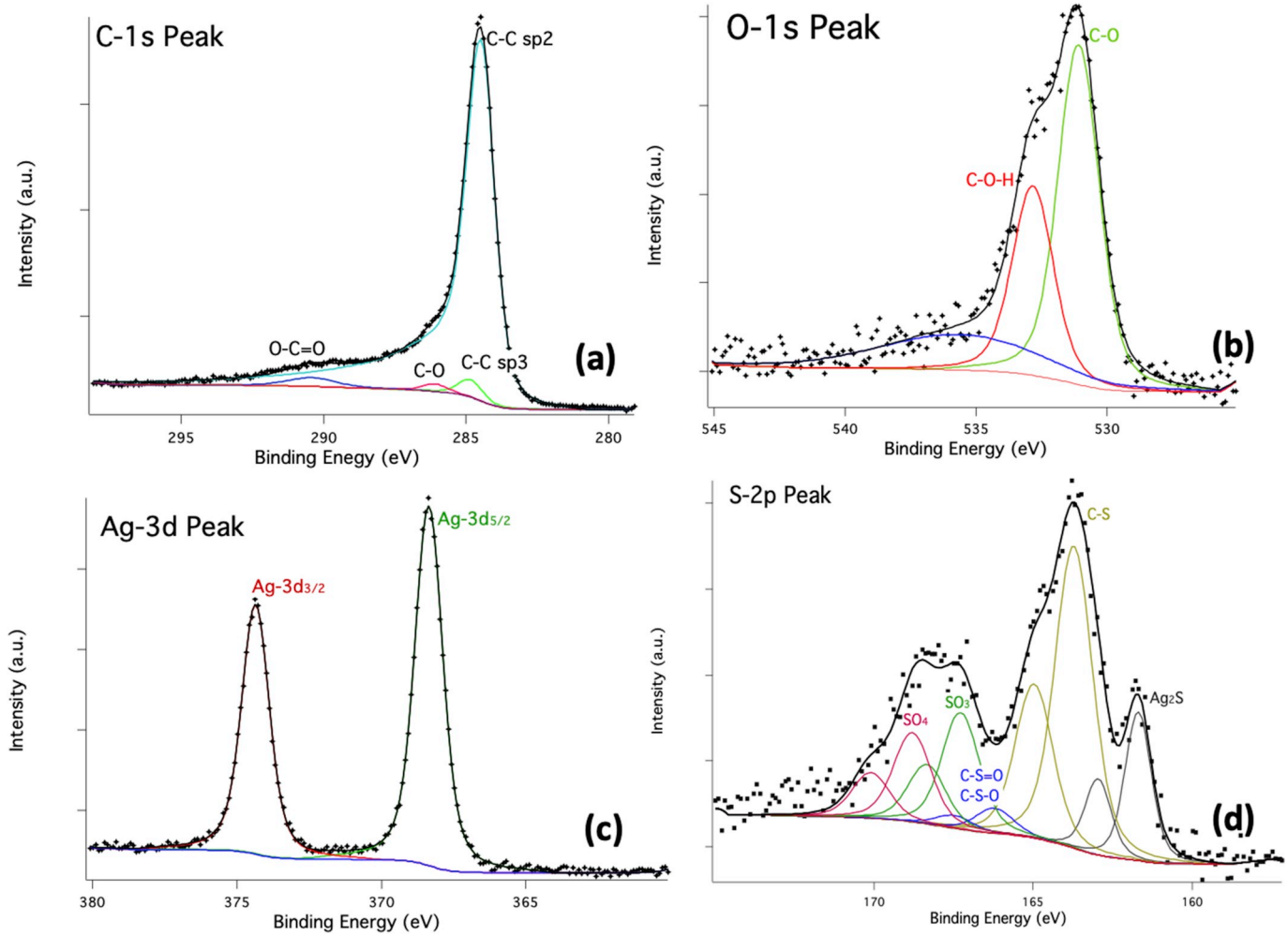

Fig. 2. XPS peak fitting results of MC-S-Ag-3 for C -1s (a); O-1s (b); Ag-3d (c); and S-2p (d) spectra.

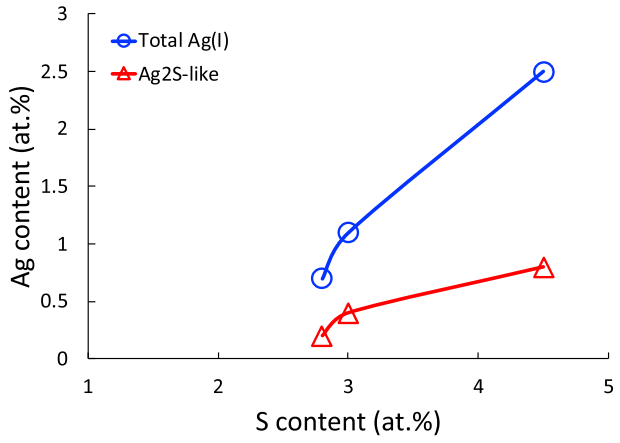

Fig. 3. Correlation of Ag (I) and S bearing functionalities present on carbon surface.

2.3. Adsorption of ethane, ethylene, propane and propylene

The adsorption isotherms of all the hydrocarbon gases, including ethane (C_2H_6), ethylene (C_2H_4), propane (C_3H_8) and propylene (C_3H_6) were measured in the same Quantachrome's Autosorb-iQ -Any gas instrument at a pressure upto 760 torr and temperature 298 K. The temperature was controlled by external chiller (Julabo®). All the gases were of ultra-high purity (UHP) grade (Air Gas).

3. Results and discussions

3.1. Materials characteristics

The elemental composition of all the Ag(I)-doped carbons is analyzed by XPS and the results are shown in Table 1. The representative peak fitting results of MC-S-Ag-3 are shown in Fig. 2(a)-(d), for C-1s, O-1s, Ag-3d and S-2p peak deconvolution, respectively. As mentioned in the table, the key elements in these composite porous carbons are carbon, oxygen, sulfur and silver. All the carbons have similar amounts of carbon and oxygen, which lie within 86–89 and 6–7 at.%. However, there is a significant change in sulfur and silver contents. Total sulfur contents increased from 2.8 to 4.5 at.% from MC-S-Ag-1 to MC-S-Ag-3, which reflected the increase in total Ag content from 0.7 to 2.5 at.%. As shown in the synthesis protocol, the large Ag(I) doped content has been caused by reacting with large amounts of $AgBF_4$. Since the total Ag content is calculated from be deconvolution of Ag-3d peak and it is not sensitive to its chemical functionalities, we tried to locate the Ag functionalities through C, O and S peak fitting results. From deconvolution of S-2p peak, it was found that there is an Ag_2S-like bond formation around 161.5 eV (Fig. 2(d)). We also concluded that there is no possible Ag–C or Ag–O like bond formation as we could not resolve the peaks at 283.5 eV and 529.5 eV from C-1 and O-1s spectra respectively, that are representatives of those functionalities. Furthermore, XPS results also confirmed that there is no metallic Ag(0) in any of the carbons as Ag-3d peak pattern did not show any satellite peak at around 372 eV. Furthermore, as XPS results did not find B or F in the overall scan, the possibility of remaining $AgBF_4$ in the system can be ruled out. Most likely, the Ag functionalities other than Ag_2S type is the physiosorbed Ag (I) in the pores of the carbons, probably, in the proximity of sulfur bearing functionalities. Fig. 3 shows the nature of monotonic increase of Ag(I) functionalities with the increase in S functionalities in those carbons, which corroborates the well-known fact of high affinity silver towards sulfur functionalities.

Table 2
Pore textural properties.

Carbon species	BET SSA (m^2/g)	Micropore volume (cm^3/g)	Total pore volume (cm^3/g)
MC-S-Ag-1	915	0.39	0.48
MC-S-Ag-2	797	0.32	0.43
MC-S-Ag-3	1193	0.43	0.58

The N_2 adsorption-desorption plot at 77 K is shown in Fig. 4(a). Pore textural properties are shown in Table 2. It is observed that MC-Ag-S3 has the highest BET specific surface area of 1193 m^2/g followed by MC-Ag-S1 and MC-Ag-S2. Micropore and total pore volume follow the same trend. The pore size distribution is calculated by using non-local density function theory (NLDFT) by combining the N_2 adsorption at 77 K and CO_2 adsorption at 273 K. CO_2 adsorption isotherms and cumulative pore size distribution plots are given in supporting information (Figs. S1 and S2). As observed in differential pore size distribution plot (Fig. 4(b)), all the carbons have distinct ultramicropore size at around 5.2 and 8.2 Å and a larger micropore size in the range of 16–17 Å. All the carbons also have a very small and distributed mesopore contributions in the range of 20–35 Å that might cause the small hysteresis loop in the N_2 adsorption-desorption plot as shown in Fig. 4(a). It needs to be mentioned that as the selectivity towards alkene is only demonstrated by MC-S-Ag-3, which has the highest Ag(I) content, we performed the remaining materials characteristics studies (SEM-EDX) for this material

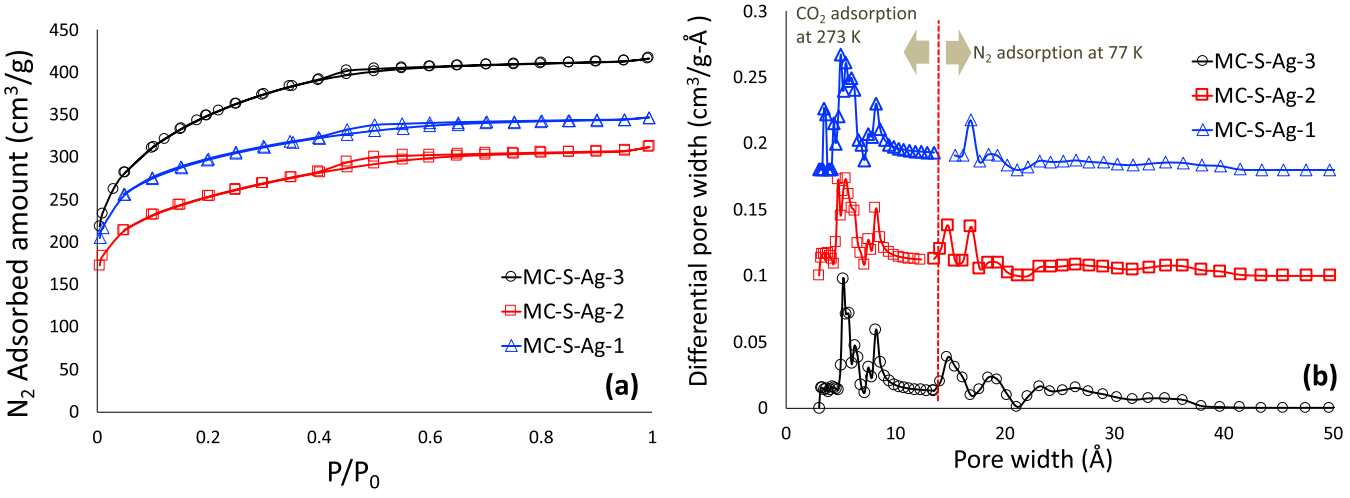

Fig. 4. N_2 adsorption-desorption isotherms at 77 K (a), Differential pore size distributions (b).

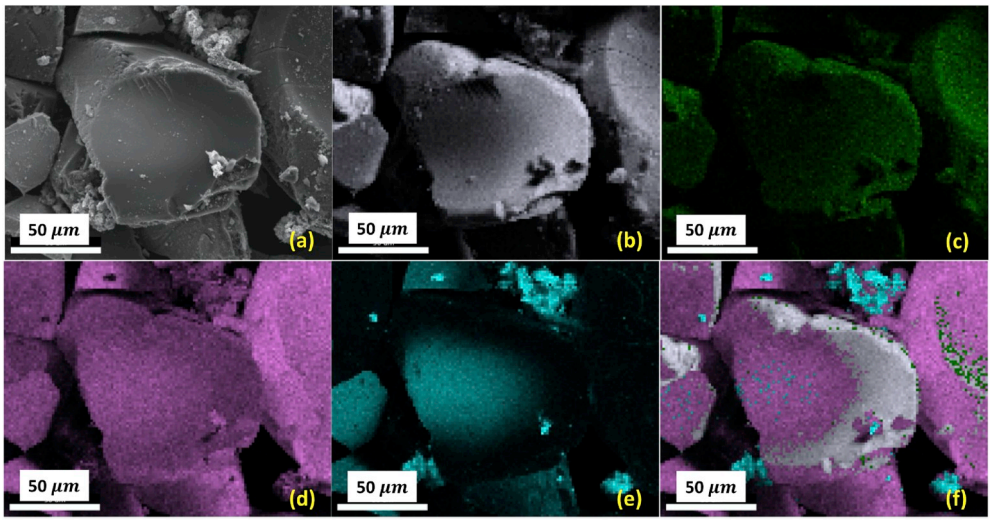

Fig. 5. SEM image of Ag(I) doped carbon (a); EDX mapping of C (b); O (c); S (d); Ag (e) and combination of C (grey), O (green), S (magenta) and Ag (blue) (f). (For interpretation of the references to color in this figure legend, the reader is referred to the Web version of this article.)

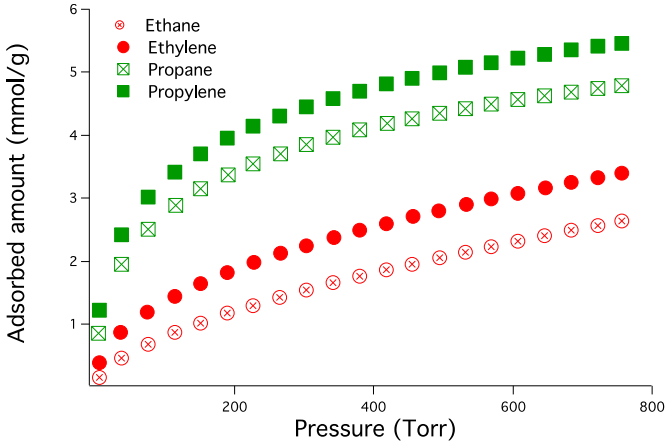

Fig. 6. Adsorption isotherms of ethane, ethylene, propane and propylene on MC-S-Ag-3 at 298 K.

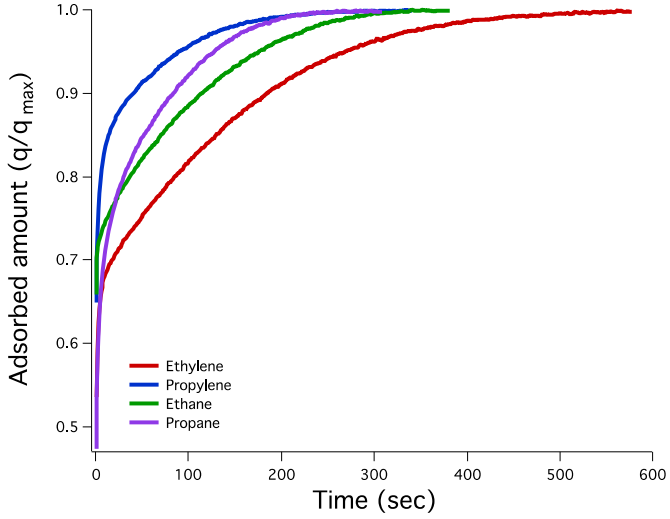

Fig. 7. Kinetics of adsorption of ethane, ethylene, propane and propylene on MC-S-Ag-3 at 298 K.

only.

SEM images and the corresponding EDX mapping images are shown in Fig. 5(a)-(f). It was observed that particle shapes and sizes were irregular with particle size in the range of 25–150 μm. The EDX mapping was performed for C (Fig. 5(b)), O (Fig. 5(c)), S (Fig. 5(d)) and Ag (Fig. 5 (e)) and combination of all the elements (Fig. 5(f)). The mapping shows that the distribution of these elements was almost homogeneous within the carbon matrix.

3.2. Adsorption of hydrocarbons

Adsorption isotherms of pure component ethane (C_2H_6), ethylene (C_2H_4), propane (C_3H_8) and propylene (C_3H_6) at 298 and pressure upto 760 torr for MC-S-Ag-3 are shown in Fig. 6. As observed, the ethylene and propylene adsorption amount at all pressures is higher than that of ethane and propane, respectively, suggesting the selectivity of this adsorbent towards alkene. In this regard, it needs to be mentioned that we also performed adsorption isotherms of ethane, ethylene, propane and propylene on pristine polyfurfuryl alcohol derived activated carbon and sulfurized carbon (Figs. S3 and S4 of supporting information) and found that the selectivity of both the adsorbents towards any of the gases is negligible. As mentioned in the introduction, such selectivity is dictated by the $\pi - \pi$ complexation, which is solely caused by Ag(I) species present in the system. Furthermore, as mentioned earlier, selectivity towards alkenes is only shown by MC-S-Ag-3, which has the highest total Ag(I) in the system (2.5 at.%); other Ag(I) doped carbons did not show this specific selectivity. Most likely, Ag(I) was not high enough in those carbons to capture enough amounts of alkene by such complexation. The equilibrium uptake of ethylene and propylene in our adsorbent is about 3.4 and 5.5 mmol/g, respectively. Such adsorption capacity is higher than almost all zeolite based materials, like zeolite 5A [38], Na-ETS10 [26], or NaX [4], silica, like HMS [39] or Ag-SBA-15 [11,40] and boron nitride [24]. This adsorption capacity is also higher than a large array of metal organic frameworks (MOFs), including UTSA-30 [41], 33 [42] and 35 [43], ZIF-7 [44] and 8 [45], and Cr or Cu-MIL-101 [46] or Cr-MIL-101-SO_3Ag [28]. The alkane-alkene adsorption in carbon-based materials is extremely limited [47] and demonstrates its very poor selectivity to either of alkane and alkene. The kinetics of adsorption of ethane, ethylene, propane and propylene are shown Fig. 7. It is observed that the kinetics of an alkene is sluggish compared to that of corresponding alkane, which could have been caused by interaction with Ag(I) present on the adsorbent. We could not compare the nature of kinetics of alkane and alkene with other Ag

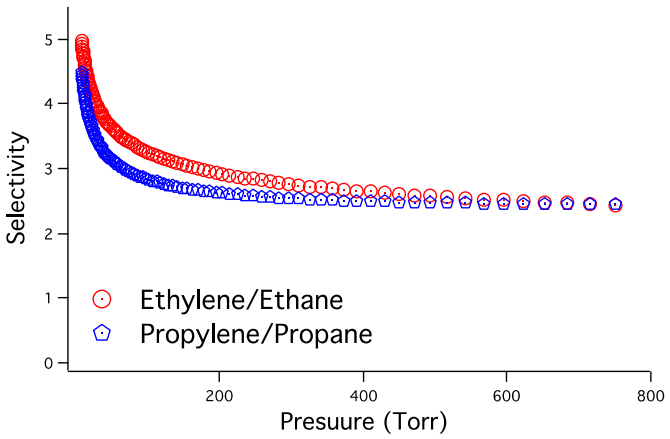

Fig. 8. Results of IAST selectivity of ethylene/ethane and propylene/propane /on MC-S-Ag-3

(I)-doped species due to the lack of such data in literature.

Owing to the difficulty in performing the mixed adsorption, it is a common practice in gas separation studies to perform the pure component adsorption and report the possible separation by selectivity values. The selectivity signifies the preference of the adsorption one component over other in a binary mixture. The selectivity of component (1) (preferred component) over (2) (non-preferred component) is defined as,

$$S_{1/2} = \frac{x_1/y_1}{x_2/y_2} \tag{1}$$

Where, x and y are the adsorbed and bulk phase compositions of (1) and (2), respectively.

The selectivity is calculated by the Ideally Adsorbed Solution Theory (IAST). The IAST-based selectivity of ethylene/ethane and propylene/propane in their respective 50/50 vol% mixtures are shown in Fig. 8. While calculating the IAST-based selectivity, the pure component isotherms were model fitted with the Sips (Langmuir-Freundlich) model. The model equation and the data fitting parameters are given in the supporting information (Table S1). The selectivity values for ethylene/ethane and propylene/propane lie within 5–2.4 and 4.5-2.4, respectively for 7–100 torr pressure. These selectivity values are higher than few zeolites, like zeolite 5A [38], few cation exchanged ETS-10 [26], and large array of metal-organic frameworks (MOFs), like UTSA-30 [41], 33 [42] and 35 [43], HKUST-1 [48], ZIF-7 [44] and 8 [45], IRMOF-8, MAF-49, $Fe_2(O_2)$(dobdc), Ni(bdc)(ted)$_{0.5}$ or Cr(MIL)-101 [49]. However, few MOFs with open metal center or unsaturated metal sites, like Fe-MIL-100 [50], Fe-MOF-74 [51], Co-MOF-74 [51] and Ag(I) doped MOF, like PAF-1-SO_3-Ag is reported to reach extremely high selectivity values. The maximum selectivity values for ethylene/ethane is observed to exceed 100 for PAF-1-SO_3-Ag [29] and the same values for propylene/propane is observed to reach 30 for Cr-MIL-101-SO_3Ag [28]. Nonetheless, to the best of our knowledge, this work is the first reported carbon-based adsorbent, which is selective towards alkene in the alkane-alkene mixture and may possibly open the door for next generation of carbon-based adsorbents for separation and purification of alkenes.

As we demonstrated in our previous publications [34,37,52] using the same IAST theory, it is also feasible to calculate binary adsorption isotherms from the experimental pure component adsorption isotherms [24,34,35,37]. The binary adsorption isotherm for component (1) and (2) can be calculated from the following equations,

$$q_1 = x_1 q \tag{2}$$

and

$$q_2 = x_2 q \tag{3}$$

Where q is the total adsorbed amount and can be calculated from the IAST theory as

$$\frac{1}{q} = \frac{x_1}{q_1^*} + \frac{x_2}{q_2^*} \tag{4}$$

Where, q_1^* and q_2^* correspond to the adsorbed amounts of the pure component gases at the same temperature and spreading pressure or surface potential as that of adsorption mixture. The simulated binary adsorption isotherms are shown in Fig. 9(a) and (b), respectively.

Separation of gases can be well demonstrated by transient column breakthrough curves. Owing to the heavy instrumentation and large volume of adsorbent materials requirements, it is also a common practice to simulate the transient breakthrough time based on the pure component adsorption data. Transient breakthrough simulations were carried out for binary (50/50 vol%) C_2H_4/C_2H_6, and C_3H_6/C_3H_8 feed mixtures in MC-Ag-S-3, operating at a total pressure of 100 kPa and 298 K, using the methodology described in earlier publications [53–56]. The breakthrough simulations were performed using in-house custom-built code. For the breakthrough simulations, the parameter values that were used are length of packed bed, $L = 0.3$ m; voidage of packed bed, $\varepsilon = 0.4$; and superficial gas velocity at inlet, $u = 0.04$ m/s. The simulated transient breakthrough plots for C_2H_4/C_2H_6, and 50/50 C_3H_6/C_3H_8 mixtures are shown in Fig. 10(a) and (b). In those figures, the y-axis is the dimensionless concentrations of each component at the exit of the fixed bed, normalized with respect to the inlet feed concentrations (C_i/C_{i0}). The x-axis is the dimensionless time, $\tau = \frac{tu}{L\varepsilon}$, defined by dividing the actual time, t, by the characteristic time, $\frac{L\varepsilon}{u}$. The breakthrough

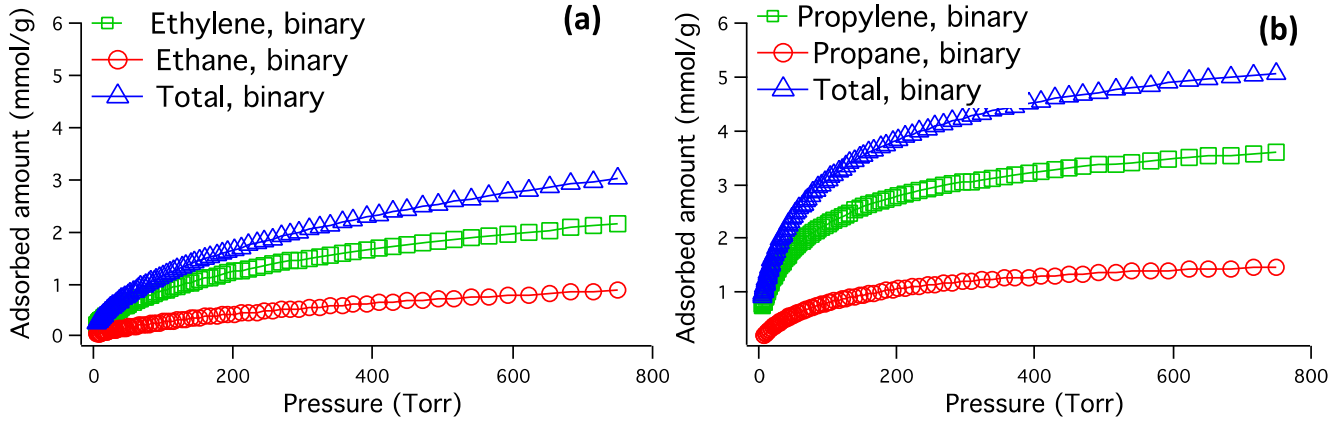

Fig. 9. IAST-based simulated binary adsorption isotherms of ethane and ethylene (a); and propane and propylene (b) on MC-S-Ag-3.

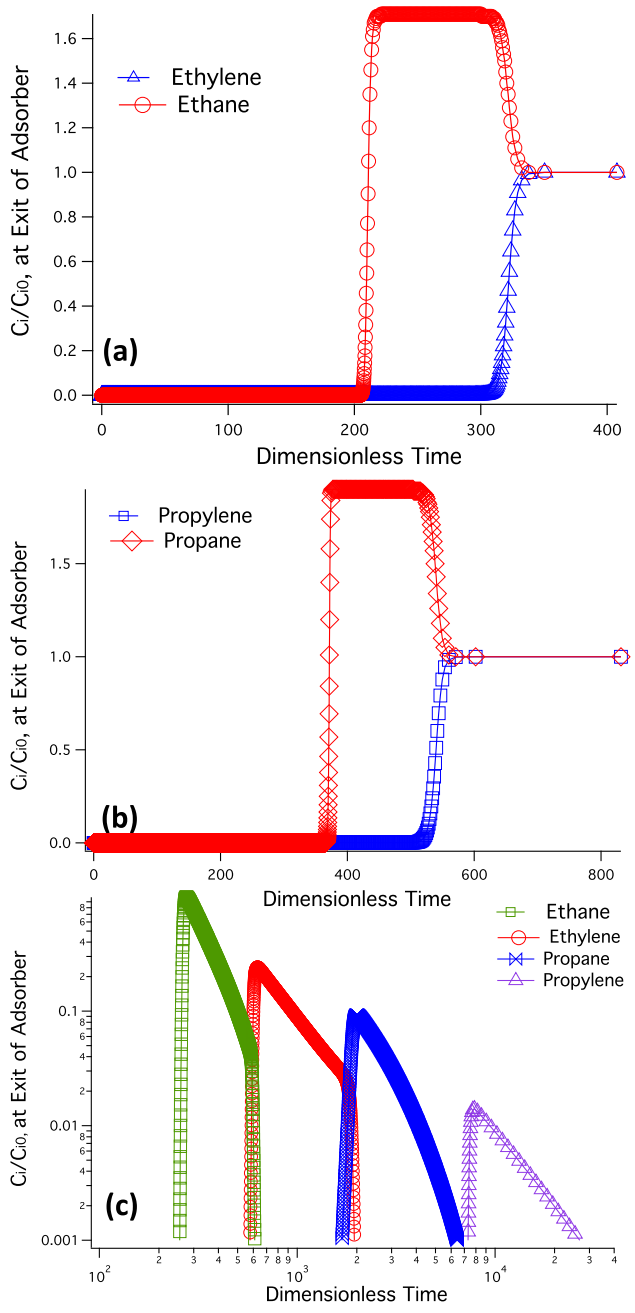

Fig. 10. Simulated breakthrough plots for ethane-ethylene (a) and propane-propylene (b) for 50-50 mol% feed mixtures Simulated pulse chromatographic plot for equimolar mixture of ethane, ethylene, propane and propylene (c).

simulations demonstrate the potential of producing purified product gas C_2H_4 and C_3H_8 during the time interval in between breakthrough the of C_2H_4/C_2H_6 and C_3H_6/C_3H_8. In addition to breakthrough simulation, we also performed a pulse chromatographic simulation with equimolar four component mixture consisting of ethane, ethylene, propane and propylene in order to simulate the possible separation of these hydrocarbon mixtures coming from fluid catalytic cracker (FCC) unit of the laboratory. As shown in Fig. 10(c), the pulses appear in the sequence of ethane, ethylene, propane and propylene, which are exactly in the same order of their equilibrium adsorption amounts as shown in Fig. 6. It also appears that these individual components are separated from each other with no practical overlap. It implies that this carbon is also capable of fractionating a four-component mixture into four individual components.

4. Conclusions

In this phase of research, we have successfully synthesized sulphurated and Ag(I) doped microporous carbons from furfuryl alcohol as carbon precursor. The Ag(I) content of the carbons demonstrated the monotonic relation with sulfur content thereby signifying the affinity of sulfur towards silver. All the resultant carbons were successfully characterized with pore textural properties, SEM-EDX and XPS. The BET specific surface areas of the carbons lied within 915–1193 m^2/g along with Ag(I) content of 0.7–2.5 at.%. Adsorption studies suggested only the carbon with highest Ag(I) content demonstrated affinity towards alkene, i.e., ethylene and propylene over ethane and propane, respectively. The IAST-based selectivity values for ethylene/ethane and propylene/propane lie within 4.5 to 2.5 and 5 to 2.4, respectively. IAST-based values were also employed to calculate binary adsorption isotherms, column breakthrough and pulse chromatography. The overall results suggested that these carbons can be considered as potential candidates for light olefin separation from their alkane counterparts.

Declaration of competing interest

None.

CRediT authorship contribution statement

Dipendu Saha: Conceptualization, Funding acquisition, Investigation, Methodology, Project administration, Supervision, Writing - original draft. **Brandon Toof:** Data curation, Methodology. **Rajamani Krishna:** Software, Conceptualization. **Gerassimos Orkoulas:** Software, Conceptualization. **Pasquale Gismondi:** Data curation, Methodology. **Ryan Thorpe:** Data curation. **Marisa L. Comroe:** Data curation, Methodology.

Acknowledgement

This work was funded by American Chemical Society sponsored Petroleum Research Fund (ACS-PRF) with grant no. 59667-UR10. D.S. and G.O. acknowledges the partial support from Faculty Development Award from Widener University. B.T. acknowledges the support from School of Engineering of Widener University.

Appendix A. Supplementary data

Supplementary data to this article can be found online at https://doi.org/10.1016/j.micromeso.2020.110099.

References

[1] D.S. Sholl, R.P. Lively, Nature 352 (2016) 435–437, https://doi.org/10.1038/532435a.
[2] D. Saha, H. Grappe, A. Chakraborty, G. Orkoulas, Chem. Rev. (2016) 11436–11499, https://doi.org/10.1021/acs.chemrev.5b00745.
[3] J.A. Moulijn, M. Makkee, A. van Diepen, Chemical Process Technology, John Wiley & Sons, Chichester, England), 2001.
[4] A. V. Miltenburg, W. Zhu, F. Kapteijn, J. A. Moulijn, Chem. Eng. Res. Des., 84(A5): 350–354. . https://doi.org/10.1205/cherd05021.
[5] S. Matar, L.F. Hatch, Chemistry of Petrochemical Processes, second ed., Gulf Publishing Company, Texas, 2000.
[6] A.M. Aitani, Oil Gas Eur. Mag. 30 (2004) 36–39.
[7] J.A. Moulijn, M. Makkee, A. van Diepen, Chemical Process Technology, John Wiley & Sons, Chichester, England, 2001.
[8] R.A. Buyanov, N.A. Pakhomov, Kinet. Catal. 41 (2001) 64–75, https://doi.org/10.1023/A:1004852829938.
[9] G.R. Kotelnikov, S.M. Komarov, V.I. Titov, V.P. Bespalov, Petrol. Chem. 41 (2001) 422–427.
[10] H. Weyten, J. Luyten, K. Keizer, L. Willems, R. Leysen, Catal. Today 56 (2000) 3–11, https://doi.org/10.1016/S0920-5861(99)00257-6.

[11] C.A. Grande, J.D.P. Araujo, S. Cavenati, N. Firpo, E. Basaldella, A.E. Rodrigues, Langmuir 20 (2004) 5291–5297, https://doi.org/10.1021/la036400s.
[12] X. Wang, Y. Wu, J. Peng, Y. Wu, J. Xiao, Q. Xia, Z. Li, Chem. Eng. J. 358 (2019) 1114–1125, https://doi.org/10.1016/j.cej.2018.10.109.
[13] R.B. Eldridge, Ind. Eng. Chem. Res. 22 (1993) 2208, https://doi.org/10.1021/ie00022a002.
[14] R.A. Meyers, Handbook of Petroleum Refining Processes, McGraw Hill, New York, 2003, p. 900.
[15] F.G. Kerry, Industrial Gas Handbook: Gas Separation and Purification, CRCPress, Boca Raton, FL, 2007.
[16] D. Banerjee, J. Liu, P.K. Thallapally, Comments Mod. Chem. 35 (2015) 18–38, https://doi.org/10.1080/02603594.2014.976704.
[17] J.W. Yoon, I.T. Jang, K.-Y. Lee, Y.K. Hwang, J.-S. Chang, Korean Chem. Soc. 31 (2010) 220–223, https://doi.org/10.5012/bkcs.2010.31.01.220.
[18] J.L. Humphrey, A.F. Seibert, R.A. Koort, Separations technologies advances and priorities, in: U.S. Department of Energy Report 12920-1, 1991.
[19] X. Wang, Y. Wu, X. Zhou, J. Xiao, Q. Xia, H. Wang, Z. Li, Chem. Eng. Sci. 155 (2016) 338–347, https://doi.org/10.1016/j.ces.2016.08.026.
[20] X. Zhu, C. Tian, S.M. Mahurin, S.H. Chai, C. Wang, S. Brown, G.M. Veith, H. Luo, H. Liu, S. Dai, J. Am. Chem. Soc. 134 (2012) 10478–10484, https://doi.org/10.1021/ja304879c.
[21] J. Ploegmakers, S. Japip, K. Nijmeijer, J. Membr. Sci. 428 (2013) 331–340, https://doi.org/10.1021/ja304879c.
[22] J. Hou, P. Liu, M. Jiang, L. Yu, L. Li, Z. Tang, J. Mater. Chem. A 7 (2019) 23489–23511, https://doi.org/10.1039/C9TA06329C.
[23] D.J. Safarik, R.B. Eldrige, Ind. Eng. Chem. Res. 37 (1998) 2571–2581, https://doi.org/10.1021/ie970897h.
[24] D. Saha, G. Orkoulas, S. Yohannan, H.-C. Ho, E. Cakmak, J. Chen, S. Ozcan, ACS Appl. Mater. Interfaces 9 (2017) 14506–14517, https://doi.org/10.1021/acsami.7b01889.
[25] S. Aguado, G. Bergeret, C. Daniel, D. Farrusseng, J. Am. Chem. Soc. 36 (2012) 14635–14637, https://doi.org/10.1021/ja305663k.
[26] A. Anson, Y. Wang, C.C.H. Lin, T. M Kuznicki, S.M. Kuznicki, Chem. Eng. Sci. 63 (2008) 4171–4175, https://doi.org/10.1016/j.ces.2008.05.038.
[27] Adsorptive separation of light olefin/paraffin mixtures, PhD dissertation, in: Dispersion of CuCl in Faujasite Zeolites, Arjen Van Miltenburg, Sep 2007.
[28] G. Chang, M. Huang, Y. Su, H. Xing, B. Su, Z. Zhang, Q. Yang, Y. Yang, Q. Ren, Z. Bao, Chem. Commun. 51 (2015) 2859–2862, https://doi.org/10.1039/C4CC09679G.
[29] B. Li, Y. Zhang, R. Krishna, K. Yao, Y. Han, Z. Wu, D. Ma, Z. Shi, T. Pham, B. Space, J. Liu, P.K. Thallapally, J. Liu, M. Chrzanowski, S. Ma, J. Am. Chem. Soc. 136 (2014) 8654–8660, https://doi.org/10.1021/ja502119z.
[30] F.J. Blas, V.F. Vega, K.E. Gubbins, Fluid Phase Equil. 150 (1998) 117–124, https://doi.org/10.1016/S0378-3812(98)00282-9.
[31] C.A. Grande, N. Firpo, E. Basaldella, A.E. Rodrigues, Adsorption 11 (2005) 775–780, https://doi.org/10.1007/s10450-005-6022-4.
[32] D. Banerjee, J. Liu, P.K. Thallapally, Comments Mod. Chem. 35 (2015) 18–38, https://doi.org/10.1080/02603594.2014.976704.
[33] D. Saha, C.I. Contescu, N.C. Gallego, Langmuir 28 (2012) 5669–5677, https://doi.org/10.1021/la3002948.
[34] D. Saha, R. Thorpe, S.E. Van Bramer, N. Alexander, D. Hensley, G. Orkoulas, J. Chen, ACS Omega 3 (2018) 18592–18602, https://doi.org/10.1021/acsomega.8b02892.
[35] D. Saha, B. Taylor, N. Alexander, D.F. Joyce, G.I. Faux, Y. Lin, V. Shteyn, G. Orkoulas, Bioresour. Technol. 256 (2018) 232–240, https://doi.org/10.1016/j.biortech.2018.02.026.
[36] D. Saha, S. Barakat, S. Van Bramer, K.A. Nelson, D.K. Hensley, J. Chen, ACS Appl. Mater. Interfaces 8 (2016) 34132–34142, https://doi.org/10.1021/acsami.6b12190.
[37] D. Saha, G. Orkoulas, J. Chen, D.K. Hensley, Microporous Mesoporous Mater. 241 (2017) 226–237, https://doi.org/10.1016/j.micromeso.2016.12.015.
[38] M. Mofarahi, S.M. Salehi, Adsorption 19 (2013) 101, https://doi.org/10.1007/s10450-012-9423-1.
[39] B.L. Newalkar, N.V. Choudary, U.T. Turaga, R.P. Vijayalakshmi, P. Kumar, S. Komarneni, T.S.G. Bhat, Microporous Mesoporous Mater. 65 (2003) 267–276, https://doi.org/10.1016/j.micromeso.2003.08.008.
[40] C. Grande, N. Firpo, E. Basaldella, A. Rodrigues, Adsorption 11 (2005) 775–780, https://doi.org/10.1007/s10450-005-6022-4.
[41] Y. He, S. Xiang, Z. Zhang, S. Xiong, F.R. Fronczek, R. Krishna, M. O'Keeffe, B. Chen, Chem. Commun. 48 (2012) 10856–10858, https://doi.org/10.1039/C2CC35729A.
[42] Y. He, Z. Zhang, S. Xiang, F.R. Fronczek, R. Krishna, B. Chen, Chem. Eur J. 18 (2011) 613–619, https://doi.org/10.1002/chem.201102734.
[43] Y. He, Z. Zhang, S. Xiang, F.R. Fronczek, R. Krishna, B. Chen, Chem. Commun. 48 (2012) 6493, https://doi.org/10.1039/C2CC31792C.
[44] C. Gucuyener, V.D. Bergh, J. Gascon, F. Kapteijn, J. Am. Chem. Soc. 132 (2010) 17704–17706, https://doi.org/10.1021/ja1089765.
[45] U. Böhme, B. Barth, C. Paula, A. Kuhnt, W. Schwieger, A. Mundstock, J. Caro, M. Hartmann, Langmuir 29 (2013) 8592–8600, https://doi.org/10.1021/la401471g.
[46] G. Chang, Z. Bao, Q. Ren, S. Deng, Z. Zhang, B. Su, H. Xing, Y. Yang, RSC Adv. 4 (2014) 20230–20233, https://doi.org/10.1039/c4ra02125h.
[47] E. Costa, G. Calleja, C. Marrbn, A. Jimenez, J. Pau, J. Chem. Eng. Data 34 (1989) 156–160, https://doi.org/10.1021/je00056a003.
[48] Y. He, R. Krishna, B. Chen, Energy Environ. Sci. 5 (2012) 9107–9120, https://doi.org/10.1039/C2EE22858K.
[49] L. Li, R.-B. Lin, R. Krishna, H. Li, S. Xiang, H. Wu5, J. Li1, W. Zhou, B. Chen, Science 362 (2018) 443–446, https://doi.org/10.1126/science.aat0586.
[50] J.W. Yoon, Y.-K. Seo, Y.K. Hwang, J.-S. Chang, H. Leclerc, S. Wuttke, P. Bazin, A. Vimont, M. Daturi, E. Bloch, P.L. Llewellyn, C. Serre, P. Horcajada, J.-M. Greneche, A.E. Rodrigues, G. Ferey, Angew. Chem. Int. Ed. 49 (2010) 5949–5952, https://doi.org/10.1002/anie.201001230.
[51] P. Li, Y. He, H.D. Arman, R. Krishna, H. Wang, L. Weng, B. Chen, Chem. Commun. 50 (2014) 13081–13084, https://doi.org/10.1039/C4CC05506C.
[52] D. Saha, B. Taylor, N. Alexander, D.F. Joyce, G.I. Faux, Y. Lin, V. Shteyn, G. Orkoulas, Bioresour. Technol. 256 (2018) 232–240, https://doi.org/10.1016/j.biortech.2018.02.026.
[53] R. Krishna, Microporous Mesoporous Mater. 185 (2014) 30–50, https://doi.org/10.1016/j.micromeso.2013.10.026.
[54] R. Krishna, RSC Adv. 5 (2015) 52269–52295, https://doi.org/10.1039/C5RA07830J.
[55] R. Krishna, RSC Adv. 7 (2017) 35724–35737, https://doi.org/10.1039/C7RA07363A.
[56] R. Krishna, Separ. Purif. Technol. 194 (2018) 281–300, https://doi.org/10.1016/j.seppur.2017.11.056.

Supporting Information

Separation of Ethane-Ethylene and Propane-Propylene by Ag(I) Doped and Sulfurized Microporous Carbon

Dipendu Saha[1],*, Brandon Toof[1], Rajamani Krishna[2], Gerassimos Orkoulas[1],Pasquale Gismondi[1], , Ryan Thorpe[3], Marisa Comroe[1]

[1] Department of Chemical Engineering, Widener University, One University Place, Chester, PA 19013, [2.]Van't Hoff Institute for Molecular Sciences, University of Amsterdam, Science Park 904, 1098 XH Amsterdam, The Netherlands [3]Department of Physics and Astronomy, Rutgers University, Piscataway, NJ 08854, USA

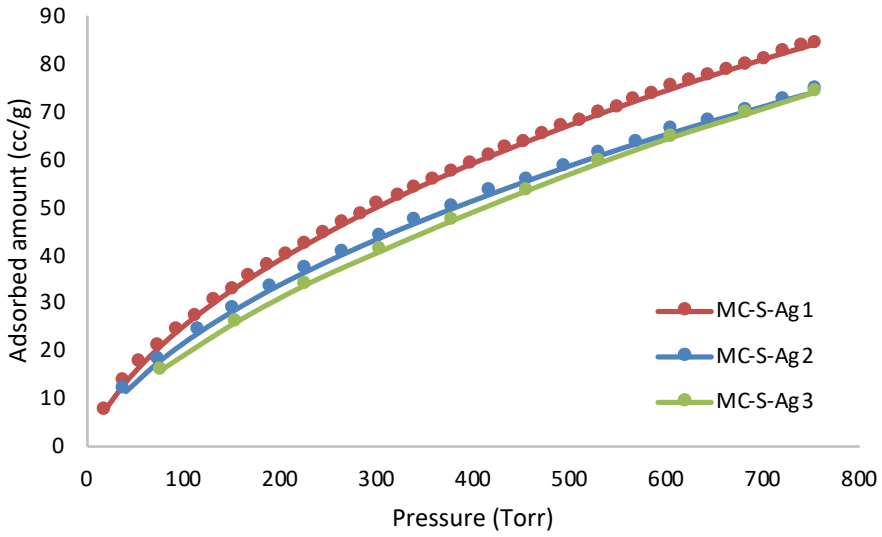

Figure S1. CO_2 adsorption isotherms at 273 K.

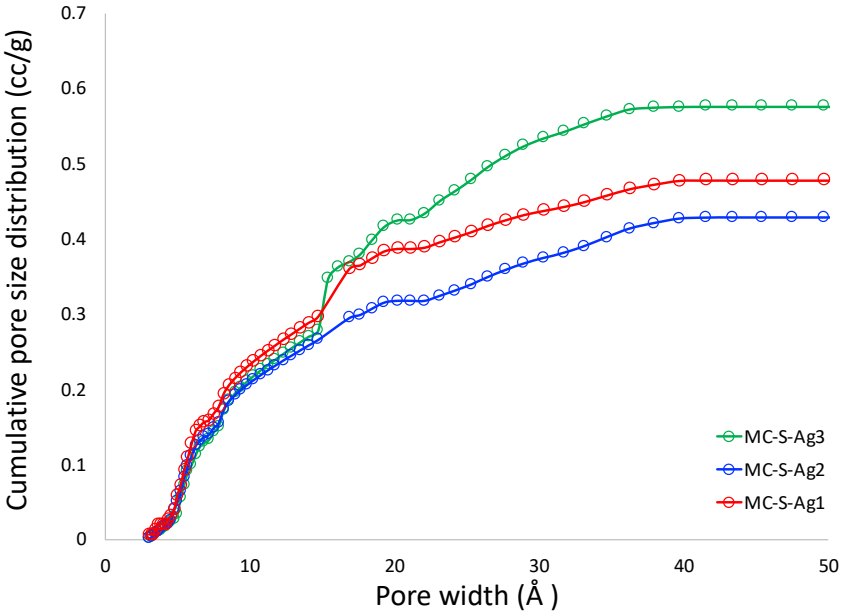

Figure S2. Cumulative pore size distribution plot

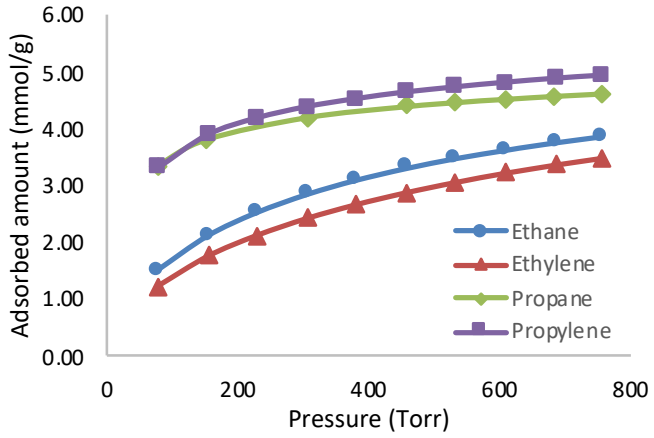

Figure S3. Adsorption isotherms of ethane, ethylene propane and propylene on pristine polyfurfuryl alcohol derived activated carbon

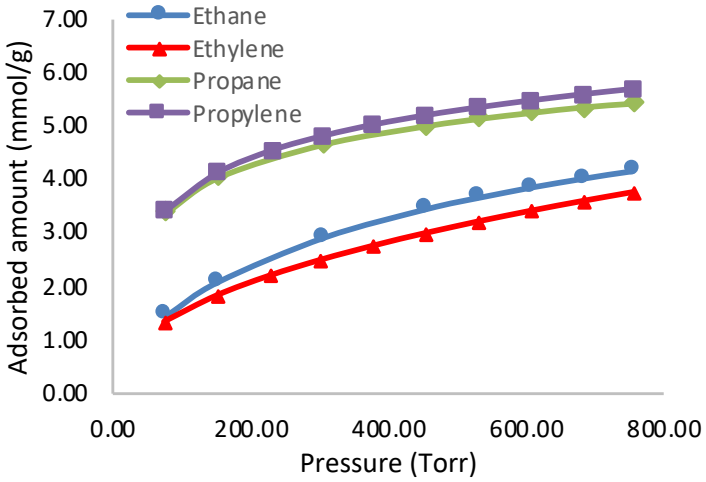

Figure S4. Adsorption isotherms of ethane, ethylene propane and propylene on sulfurized polyfurfuryl alcohol derived activated carbon

SIPS equation:

$$q = q_{sat} \frac{bp^{\nu}}{1 + bp^{\nu}}$$

Table S1. SIPS equation constants:

	q_{sat} mmol g^{-1}	b $Pa^{-\nu}$	ν dimensionless
C_2H_4	8.6	6.3435E-04	0.6
C_2H_6	8	1.2030E-04	0.72
C_3H_6	7.1	3.0562E-03	0.6
C_3H_8	6	4.7686E-04	0.78